

Identifying Gamma-Ray Burst Remnants in Nearby Galaxies

Rosalba Perna, John Raymond and Abraham Loeb

Harvard-Smithsonian Center for Astrophysics, 60 Garden Street, Cambridge, MA 02138

ABSTRACT

We study the spectral signatures arising from cooling and recombination of an interstellar medium whose equilibrium state has been altered over ~ 100 pc by the radiation of a Gamma-Ray Burst (GRB) and its afterglow. We identify signatures in the line diagnostics which are indicative of a photo-ionized GRB remnant which is $\lesssim 5 \times 10^4$ years old. We estimate that at least a few such remnants should be detectable in the Virgo cluster of galaxies. If the γ -ray emission from GRBs is beamed to a fraction f_b of their sky, then the expected number of Virgo remnants is larger by a factor of f_b^{-1} . Virgo remnants can be resolved with arcsecond imaging, and are likely to be center-filled using narrow-band filters of high ionization lines (such as [O III] $\lambda 5007$ or He II $\lambda 4686$), and limb-brightened for low-ionization lines (such as [S II] $\lambda 6717$). The non-relativistic blast wave might be visible separately, since it does not reach the outer edge of these young photo-ionized remnants. The remnants should show evidence for ionization cones if the prompt or afterglow UV emission from GRBs is beamed.

Subject headings: gamma rays: bursts — ISM

1. Introduction

Simple synchrotron models for the afterglow emission of cosmological Gamma-Ray Burst (GRB) sources imply an ambient gas density, $\sim 1 \text{ cm}^{-3}$, which is characteristic of the interstellar medium of galaxies (e.g., Waxman 1997a,b; Wijers & Galama 1998). Indeed, direct imaging of the neighborhood of well-localized GRBs revealed faint host galaxies at cosmological distances in many cases (Bloom et al. 1999 and references therein). The detection of spectral signatures that can be associated with the GRB environment is of great interest both for distance measurements and for learning about the environment itself in which GRBs occur. A knowledge of the GRBs birthplace can help to constrain the validity of a given model for their formation. At the same time, it is also of fundamental interest to know how GRBs themselves affect their environments.

The most popular models for GRB formation currently involve either the collapse of a single massive star (the so-called “hypernova scenario” [Woosley 1993, Paczyński 1998; MacFadyen & Woosley 1998]), or the coalescence of two compact objects such as two neutron stars or a neutron

star and a black hole (Eichler et al. 1989; Narayan et al. 1992; Ruffert & Janka 1998). These models could be constrained by knowing the GRB environment. Massive stars have very short lives, thus they will explode in star-forming regions, which are typically characterized by very dense environments. On the other hand, most merging neutron stars would be very old and would have typically traveled far from their birthplace. The scenario of compact merger progenitors could thus be suggested by medium to low density environments.

We have previously shown (Perna & Loeb 1998) that the X-ray and UV components of the afterglow radiation create an ionized bubble of radius $\sim 100 \text{ pc } n_1^{-1/3}$ in the surrounding galaxy, where n_1 is the ambient density in units of 1 cm^{-3} . On a short timescale, as long as the afterglow radiation is still effective to ionize, the gradual ionization of the medium can produce time dependent absorption (Perna & Loeb 1998; Meszaros & Rees 1998) and emission lines (Ghisellini et al. 1998; Böttcher et al. 1998).

In this paper we compute the emission spectrum which results as the ionized gas slowly cools and recombines. Cooling times are typically very long, $t_{\text{cool}} \sim 10^5 (T/10^5 \text{ K}) / (n_e/1 \text{ cm}^{-3}) \text{ yr}$, at a temperature T and an electron density, n_e . If GRBs occur in galaxies, then their rate is estimated to be $\sim (10^{6-7} f_b \text{ yr})^{-1}$ (Wijers et al. 1997), where $f_b \leq 1$ is the unknown beaming factor (covering fraction) of the γ -ray emission. This implies that in every galaxy there is a non-negligible probability of finding an ionized GRB remnant at any given time. The identification of these remnants in nearby galaxies will allow a much closer study of the sites where GRBs occurred and will provide an estimate for the energy output and occurrence frequency of the events (Loeb & Perna 1998).

The hydrodynamic impact of a GRB blast wave on its environment lasts longer than the radiative ionization effect. It takes tens of millions of years for the GRB blast wave to slow down to a velocity of $\sim 10 \text{ km s}^{-1}$, at which point it may be erased by interstellar turbulence. Hence, old GRB remnants should consist of a large-size ($\sim \text{kpc}$), expanding, cold HI shell, similar to the HI supershells which were identified for two decades in nearby galaxies (Loeb & Perna 1998, Efremov, Elmegreen, & Hodge 1998; and references therein). However, it appears difficult to distinguish the old hydrodynamic remnants produced by GRBs from those produced by the accumulated effect of more conventional energy sources, such as multiple supernovae, stellar winds from OB associations, or impact from high-velocity clouds. In some cases, a class of these possibilities is disfavored. For example, recent deep CCD imaging of the HI holes in the Holmberg II galaxy (Rhode et al. 1999), did not reveal the anticipated optical emission from a normal stellar population in several of these holes, in conflict with the multiple supernova or stellar wind interpretations. Nevertheless, even in this case, the old age of the hydrodynamic remnants does not allow for a unique identification of GRBs as their energy sources. On the other hand, since the energy release in GRB remnants is impulsive, it should be easier to distinguish them from conventional sources by identifying their unique spectral signatures at a sufficiently early time when they are *young* and radiant. As we show later, the emission from young GRB remnants with ages of $\lesssim 10^4$ years is affected mostly by the radiative ionization effect of the early GRB afterglow on its surrounding interstellar

medium, since it takes much more than 10^4 years for the non-relativistic blast wave to traverse the photoionized region. The impulsive energy release of hard ionizing radiation is unique to GRB sources and could distinguish young GRB remnants from the remnants of multiple supernovae.

The goal of this paper is to identify the spectral signatures that are peculiar to GRB remnants and that can be distinguished from those due to the remnants of other explosive events, such as supernovae. In §2 we present the computational scheme adopted for this problem. In §3 we show our numerical results, and analyze the particular spectral signatures of young GRB remnants. In §4 we consider the expected effect of variations in the input parameters used in our calculations. Finally, §5 summarizes our main conclusions.

2. Model Assumptions and Computational Scheme

We consider a GRB source which turns on at time $t = 0$ and illuminates a stationary ambient medium of uniform density n , with a time dependent luminosity per unit frequency, $L_\nu(t)$. The release in the surrounding medium of a large amount of ionizing radiation is a distinctive feature of GRBs and their afterglows, as opposed to supernova explosions, where any impulsive electromagnetic release would not escape promptly, but would be degraded by adiabatic expansion of the envelope before it could leak out. In our work, we limit our analysis to the effects of the afterglow photoionizing radiation on the medium. The blast wave lags behind the ionizing front, and until the time it reaches larger radii, from which most of the absorption and reemission comes, it is not expected to greatly affect the ionization state of the medium and the resulting luminosity. We will discuss this point in greater detail in §3.

Afterglows are most naturally explained by models in which the bursts are produced by relativistically expanding fireballs (Paczynski & Rhoads 1993; Meszaros & Rees 1997; Vietri 1997a; Waxman 1997a,b; Wijers, Rees, & Meszaros 1997; Vietri 1997b; Sari 1997). On encountering an external medium, the relativistic shell which emitted the initial GRB decelerates and converts its bulk kinetic energy to synchrotron radiation, giving rise to the afterglow. The combined radio and optical data imply that the fireball energy is $\sim 10^{51-52}$ erg. In the simplest unbeamed synchrotron model (e.g., Waxman 1997a,b), the time and frequency dependence of the afterglow luminosity is given by

$$L_\nu(t) = L_{\nu_m} \left(\frac{\nu}{\nu_m(t)} \right)^{-\alpha}, \quad (1)$$

where,

$$\nu_m(t) = 1.7 \times 10^{16} \left(\frac{\xi_e}{0.2} \right)^2 \left(\frac{\xi_B}{0.1} \right)^{1/2} E_{52}^{1/2} t_{\text{hr}}^{-3/2} \text{ Hz}. \quad (2)$$

Here ξ_B and ξ_e are the fractions of the equipartition energy in magnetic field and accelerated electrons, $E = 10^{52} E_{52}$ erg is the fireball energy, $t_{\text{hr}} \equiv (t/\text{hr})$, and

$$L_{\nu_m} = 8.65 \times 10^{29} \sqrt{n_1} \left(\frac{\xi_B}{0.1} \right) E_{52} \text{ erg s}^{-1} \text{ Hz}^{-1}, \quad (3)$$

where n_1 is the ambient proton density in units of 1 cm^{-3} . The spectral index α is chosen to have the values $\alpha_1 = -1/3$ for $\nu \leq \nu_m$ and $\alpha_2 = 0.7$ for $\nu > \nu_m$, so as to match the temporal decay slope observed for GRB 970228 (Fruchter et al. 1998) and GRB 970508 (Galama et al. 1998).

We consider a uniform medium which is initially neutral and in thermodynamic equilibrium, with a temperature $T \sim 10^4 \text{ K}$, and include all the most important astrophysical elements, that is H, He, C, N, O, Ne, Mg, Si, S, Ar, Ca, Fe, Ni. Their abundances are taken from Anders & Grevesse (1989). We consider a region surrounding the GRB site of size R and medium density n , and we split it up into a radial grid with steps Δr . In propagating from a point at position r to another point at position $r + \Delta r$, the afterglow flux is reduced according to

$$F_\nu(r + \Delta r, t + \Delta t) = F_\nu(r, t) \exp[-\Delta \tau_\nu(r, t)] \frac{r^2}{(r + \Delta r)^2}, \quad (4)$$

where F_ν is in units of $\text{erg cm}^{-2} \text{ s}^{-1} \text{ Hz}^{-1}$. We denote the local number densities of the ions of the various elements by $n_a^j(r, t)$, where the superscript a characterizes the element and the subscript j characterizes the ionization state. The optical depth due to photoabsorption within the distance Δr is then given by

$$\Delta \tau_\nu(r, t) = \Delta r \sum_{a,j} n_a^j(r, t) \sigma_j^a(\nu). \quad (5)$$

The photoionization cross sections are taken from Reilman & Manson (1979). The abundances of the ions of the elements are determined by solving the system of equations

$$\frac{dn_j^a(r, t)}{dt} = q_{j-2}n_{j-2}^a + q_{j-1}n_{j-1}^a + c_{j-1}n_{j-1}^a n_e - (q_j + c_j n_e + \alpha_j n_e)n_j^a + \alpha_{j+1}n_{j+1}^a n_e. \quad (6)$$

The q_j and c_j are respectively the photoionization and collisional ionization coefficients of ion j , while α_j is the recombination coefficient. Note that q_{j-2} refers to inner shell photoionization followed by Auger ionization. The collisional ionization rates are calculated according to Younger (1981). We compute the terms due to photoionization by integrating $F_\nu \sigma_\nu$ numerically. The recombination rates are given by the sum of the radiative and dielectronic recombination rates. The radiative recombination process is the inverse of photoionization, so the rates to the ground states are computed from the photoionization cross section with the help of the detailed balance relation. Hydrogenic rates are used for radiative recombination to excited levels. The dielectronic recombination rates are taken from Burgess (1966) with modifications to take more recent calculations into account. Most important is the reduction due to autoionization to excited states (Jacobs et al. 1977), with an appropriate treatment of the weakening of this effect at higher Z (Smith et al. 1985). Since we are dealing with a non-equilibrium situation, the ionization fractions are calculated within the program. The emissivity of the medium, $E_\nu(r, t)$, is calculated by using an X-ray emission code developed by Raymond (1979), and modified with updated atomic rates, as in Cox & Raymond (1979). This code computes the spectrum of radiation emitted by a hot, optically thin plasma. The basic processes which produce the continuum radiation are bremsstrahlung, recombination and two-photon continuum. Permitted-line radiation and the

most important forbidden lines are also included, as well as the recombination-line radiation from H– and He–like ions. Photoionization heating and radiative cooling are calculated within the same code, and used to update the temperature of the plasma as a function of position and time. Compton heating and cooling of the electrons by the radiation is also taken into account, as well as the secondary effect of the radiation emitted by the gas on the gas itself. This effect is especially important during the late phase of cooling.

We start the simulation ($t = 0$) at a position $R_{\min} \ll R$, and let the afterglow flux propagate and evolve according to equation (4), while calculating, at each position $r_i \leq ct$ of the grid, the abundances of all the ions of each element, the temperature of the plasma, and the local emissivities $E_\nu(t, r_i)$. Let t_{obs} be the observer time, such that the radiation detected at $t_{\text{obs}} = 0$ corresponds to that emitted at $t = 0$ in the source frame. Then a photon emitted at position r at an angle θ with the line of sight will be detected by the observer at a time t_{obs} if it is emitted in the source frame at a time $t = t_{\text{obs}} + r \cos \theta / c$. The total emitted radiation that reaches the observer at time t_{obs} is given by

$$\begin{aligned} E_\nu^{\text{tot}}(t_{\text{obs}}) &= 2\pi \int_0^{R_{\max}} dr r^2 \int_{-1}^1 d \cos \theta E_\nu \left(r, t_{\text{obs}} + \frac{r \cos \theta}{c} \right) \\ &= 2\pi c \int_0^{R_{\max}} dr r \int_{t_{\text{obs}} - \frac{r}{c}}^{t_{\text{obs}} + \frac{r}{c}} dt E_\nu(r, t) . \end{aligned} \quad (7)$$

3. Spectral Signatures of GRB Remnants

Figure 1 depicts the temperature profile of a GRB remnant at several times. In Figure 1a we consider the situation where a GRB of energy $E = 10^{52}$ ergs occurs in a typical interstellar medium, for which we assume the density $n = 1 \text{ cm}^{-3}$. Figure 1b shows the case of a burst of the same energy occurring in a dense cloud of density $n = 10^2 \text{ cm}^{-3}$ and size $R = 10 \text{ pc}$. As the afterglow flux is proportional to \sqrt{n} [cf. Eq. (3)], the gas is heated to a higher temperature close to the source than in the lower density case. However it cools much faster than a lower density gas heated to the same temperature, because $t_{\text{cool}} \propto n^{-1}$. In both figures, the bold line shows the ionized hydrogen fraction H^+/H^0 at the times immediately following the passage of the afterglow radiation through the various shells.

Figure 2a and 2b show the emission spectrum above 13 eV at several times during cooling for the same set of parameters used in Figure 1. This ionizing flux is important for the luminosities and intensity ratios of the optical lines after the gas cools to around 10^4 K . The time behavior of some of the most important lines in the observable regions of the spectrum is shown separately in Figure 3a and 3b, again with the same set of parameters as in Figures 1 and 2. Notice how the emission from the remnant is very weak in the first tens of years, and rapidly rises when $t_{\text{obs}} \gtrsim 300 \text{ yr}$ (particularly noticeable in panels (a) and (b) of Figure 3a). This is a result of the fact that the emission to the observer starts to come from the entire volume of the remnant only when t_{obs} becomes comparable to the light crossing time R/c .

Figures 2 and 3 show that the energy from a remnant in a typical interstellar medium is mostly reemitted in the optical, UV and soft X -ray band. This is to be contrasted with the emission from a young supernova remnant, where the gas, heated by the shock to temperatures $\gtrsim 10^7\text{K}$, produces a strong emission in harder regions of the X -ray band. In the high density case, the lifetime of the emission lines is shorter, [see Figure 3b], due to the rapid cooling of the dense gas. Here, for the high density case, we considered a cloud of size 10 pc (corresponding to a column density of $3 \times 10^{21} \text{ cm}^{-2}$). Much higher column densities are not typically inferred in GRBs. In any event, for a burst which occurs in a bigger dense region, leaving a larger fraction of its energy in the surrounding medium, luminosities up to about two orders of magnitude higher than the ones shown could be observed in its remnant.

Figures 4a and 4b show the ratios between some strong optical lines as a function of time. Some important diagnostic plots commonly used to distinguish among various excitation mechanisms (Baldwin, Phillips, & Terlevich 1981; Baum, Heckman & van Brugel 1992; Dopita & Sutherland 1995) are shown in Figures 5a and 5b.

The emission–line ratios exhibited by the nebulae reflect the mechanism by which the gas is ionized and the chemical abundances and physical conditions in the line-emitting gas. If the gas is purely photoionized, the ionization state of the gas is determined primarily by the ionization parameter, defined by $U = Q(H)/4\pi r^2 n_e c$, where $Q(H)$ is the number of ionizing photons per second emitted by the source, and to a lesser extent is affected by the shape of the ionizing flux. A remarkable feature of our diagnostic plots is the generally high value of the ratio between the [O III] $\lambda 5007$ line and H_β . Numerical simulations (Shull & McKee 1979) show that such high ratios (i.e. $[\text{O III}] \lambda 5007/H_\beta \geq 5$) cannot be produced in shocks but are produced by photoionization models in which the ionization parameter is relatively high (i.e. $\sim 5 \times 10^{-3}$ for $[\text{O III}]/H_\beta \simeq 10$; this ratio increases with ionization parameter). In our case, the ionization parameter is $\gg 1$ close to the source, and is higher than $\sim 10^{-3}$ for most of the ionized gas. At early times, because of time–delay effects, the bulk of the emission comes from the region close to the source, with very high values of the ionization parameter, and this leads to correspondingly high values of $[\text{O III}] \lambda 5007/H_\beta$, not typically found in regions excited by other mechanisms. Note however that high values of $[\text{O III}] \lambda 5007/H_\beta$ are occasionally observed in supernova remnant shocks, but only during a brief period of incomplete cooling (e.g. Raymond et al. 1998), or in oxygen rich supernova remnants (e.g. Morse et al. 1996).

The ratio between [O III] $\lambda 5007$ and [O III] $\lambda 4363$ is a diagnostic of the temperature of the emitting plasma. Its increase with time is a signature of the fact that the gas is cooling. The temperature indicated is generally far higher than is observed in steady-state photoionized plasmas such as H II regions. It is even higher than is common in supernova remnants (Raymond et al. 1998) for much of the GRB cooling time.

A third commonly used line ratio diagnostic for nebulae is the $[\text{S II}] \lambda 6717,27/H_\alpha$ ratio, which is small in H II regions and planetary nebulae, and $\gtrsim 0.4$ in most shocks. A GRB remnant shows

the signatures of photoionization for most of its cooling time.

A density-diagnostic line is the [O II] $\lambda 3727,29$. An increase in the electron density generally leads to a weakening of this line. This can be seen in our case by comparing panels (d) of Figures 4a and 4b.

Perhaps the most unusual feature of the optical emission is the high ratio of He II $\lambda 4686$ to H_β . While this ratio is high for only a short time, the He II emission is extremely weak in H II regions and seldom exceeds 0.1 in supernova remnants. The strength here results from the existence of a huge volume of gas at 10^5 K or more, and the faintness of the Balmer lines at these temperatures.

In our simulation of the impact of a GRB on the external medium, we have considered only the effects of photoionization. As a matter of fact, a shock front lags behind, and we need to estimate how it affects the GRB signatures that we discussed. Needless to say, the photoionization model is only valid until the blast wave produced by the GRB event reaches the photoionized material. As long as the shocked gas is very hot, however, it will have little effect on the optical spectrum. The shock compresses the gas, thereby increasing its emissivity, but it also heats the gas. This tends to increase the energy emitted, but to decrease the number of photons produced. The blast wave will strongly affect the optical spectrum when: (a) it has swept up a substantial fraction of the photoionized gas or, (b) when the blast wave becomes radiative, producing strong ionizing radiation and strong optical emission from the cooling gas. The former case occurs when the blast wave reaches $2/3$ the radius of the photoionized region (thus reducing the volume of the optically emitting volume by 30%). The latter occurs when the shock slows to about 300 km s^{-1} , depending upon the explosion energy only as the $1/11$ power (Cox 1972).

For an explosion with an energy $E_{52} \times 10^{52}$ ergs in a uniform medium of density $n_1 \text{ cm}^{-3}$, the late phase of the blast wave evolution is described by the Sedov (1959) solution: $R \approx (19 \text{ pc})(E_{52}/n_1)^{1/5} t_4^{2/5}$, where t_4 is the time from the explosion in units of 10^4 yr . The corresponding velocity of the wave is $v \approx (750 \text{ km s}^{-1})(E_{52}/n_1)^{1/5} t_4^{-3/5}$. For an explosion with 10^{52} ergs in a medium of density n_1 , the blast wave will reach a distance of about 50 pc after $t \approx 10^6 \text{ yr}$, while the shock reaches a velocity of 300 km sec^{-1} after $t \approx 4.6 \times 10^4 \text{ yr}$. At that time, the shock has traveled a distance of about 35 pc. Let us consider the effect of the emission from the shock on a particularly important line, such as [O III] $\lambda 5007$. From the simulations of Hartigan, Raymond & Hartmann (1987), we see that the flux in the 5007 line from a shock at a velocity of 300 km sec^{-1} in a medium of density 1 cm^{-3} is $\sim 10^{-4} \text{ ergs cm}^{-2} \text{ s}^{-1}$. At a distance of 100 pc, this flux is $\sim 10^{-5} \text{ ergs cm}^{-2} \text{ s}^{-1}$ and it has to be compared with the flux from the same line due to the photoionized gas. This is on the order of $10^{38}/(4\pi r^2) \sim 10^{-4} \text{ ergs cm}^{-2} \text{ s}^{-1}$. Thus, the contribution of the shock to the emission when condition (b) is satisfied is only a few percent. The same analysis for the higher density case shows, instead, that after a time $\sim 10^4 \text{ yr}$ the optical spectrum becomes dominated by the emission from the shock.

4. Discussion

The model that we assumed for our GRB has a typical energy of 10^{52} ergs which is released isotropically, and the afterglow is produced in the standard fireball model. However, this might not always be the real scenario. A prompt optical-UV flash was detected for GRB990123 (Akerlof et al. 1999). If such a flash (coincident with the GRB and lasting for less than a minute) is generic in GRBs and carries as much energy as the gamma-ray emission (i.e. much more than the optical-UV afterglow emission), then GRBs might ionize a larger region than we previously considered. The photoionization signatures would be even stronger, and the luminosities higher. If, on the other hand, the optical-UV afterglow is beamed (and thus its energy lower than commonly estimated) then GRBs have a weaker effect on their environment and in this case it would be more difficult to distinguish them from other photoionized nebulae. A situation of non-steady state caused by photoionization, in a region where there is no evidence of a nearby photoionizing source, is however more generally typical of a GRB remnant. Unless the progenitor of a GRB is a massive star, one does not generally expect to find GRB remnants in star forming regions. On the other hand, photoionized nebulae are generally found around OB associations. Note that recently Wang (1999) has reported observations of *X*-ray emitting regions in M101 which did not show any evidence for OB associations, and has made the hypothesis that they could be associated with GRB remnants.

Other complications could arise from a non-homogeneous medium. If the medium has dense clumps in it, then these will absorb more flux than the surrounding region; they will be more luminous but will cool faster. Depending on the pressure gradient at its boundary, a dense clump may expand (and cool adiabatically), or suffer additional compression. Small clumps are more likely to be heated to a comparable temperature with respect to the surrounding medium, and thus they will expand, due to the higher pressure caused by their higher density. On the other hand, a large dense clump will absorb a considerable amount of flux, and thus it will show a much steeper temperature gradient with respect to the lower-density surrounding medium. In this case the clump might expand in one direction and be compressed in another. The time-dependence of the luminosity as a function of time in these cases would show more complicated patterns. Modelling all these secondary effects is beyond our scope, especially because the real conditions of the medium are unknown, and the possible-early production of the afterglow and its degree of beaming are as yet a subject of debate. Also, it is still far from clear whether there is a unique scenario for all the bursts, or if instead there can be substantial differences from one burst to another.

Our final discussion needs to address the issue of how many of these GRB remnants are detectable with current instruments. To this purpose, let us make some rough estimates of the possibility of detection of a strong line, say the [O III] λ 5007, for example. Its luminosity is $\gtrsim 10^{37}$ ergs s^{-1} for a time $t_L \approx 4 \times 10^4$ yr. The corresponding flux of photons at a distance $d_{\text{Mpc}} \times \text{Mpc}$ is $F_{\text{signal}} = 2 \times 10^{-2} d_{\text{Mpc}}^{-2} \text{ cm}^{-2} \text{ s}^{-1}$. The number of background sky photons for a slit of 10 Å around the 5007 Å wavelength in observations from the ground, is $F_{\text{noise}} \approx 10^{-5} \text{ cm}^{-2} \text{ s}^{-1} \text{ arcsec}^{-2}$ (Roach & Gordon 1973). For a telescope with a diameter $D = 10$ m, a spectroscopic

detection efficiency of $\epsilon = 0.1$, and an integration time of $t_{\text{int}} = 10$ hr, the signal-to-noise ratio $S/N = N_{\text{signal}} / \sqrt{N_{\text{noise}} + N_{\text{signal}}}$ obtains a value of $\sim 3.4 \times 10^5 d_{\text{Mpc}}^{-2} (1 + 2 \times 10^3 d_{\text{Mpc}}^{-2})^{-1/2}$, where $N = \epsilon F (\pi D^2 / 4) t_{\text{int}}$ is the number of photons detected if a 1" resolution element is assumed. A signal-to-noise ratio $S/N \geq 10$ will thus correspond to a maximum detection distance of $d_{\text{max}} \approx 200$ Mpc. This distance is an order of magnitude larger than the distance to the Virgo cluster of galaxies ($d_{\text{Virgo}} \approx 16$ Mpc) and is comparable to the distance of Coma cluster ($d_{\text{Coma}} \approx 10^2$ Mpc). Let us hence estimate the number of remnants that could be detected. For a population of GRBs that follow the star formation history, Wijers et al. (1997) estimated the local rate per galaxy to be $\Gamma_{\text{GRB}} = 2.5 \times 10^{-8} \text{yr}^{-1}$. Multiplying this number by t_L yields a probability of about 10^{-3} of finding a young remnant per galaxy. The number of galaxies in the Virgo cluster up to a magnitude $B=19$ is about 2500 and the total number of bright (L_*) galaxies out to a distance of 200 Mpc is $\sim 10^5$. Thus a few GRB remnants could be easily detected in the Virgo cluster, and about a hundred are detectable out to the limiting distance of 200 Mpc. We note that the above estimate is sensitive to the redshift distribution of GRBs; for example, if GRBs constitute a non-evolving population, the estimated GRB rate per galaxy is about 40 times higher (Fenimore & Bloom 1995).

If the γ -ray emission from GRBs is beamed to within a fraction f_b of their sky, then the number of remnants in Virgo would *increase* as $\Gamma_{\text{GRB}} \propto f_b^{-1}$ while the maximum number of remnants out to the limiting distance would *decrease* as $\Gamma_{\text{GRB}} d_{\text{max}}^3 \propto f_b^{1/2}$. Hence, for a relatively modest beaming factor of $f_b \lesssim 0.1$, there should be more remnants observable in Virgo than elsewhere. Moreover, Virgo remnants are easier to detect because they can be resolved, while distant remnants cannot be resolved and their flux could be easily dominated by contaminating light from their host galaxy. Based on these considerations, we conclude that an effective observational search should focus on identifying young GRB remnants in the Virgo cluster.

A photo-ionized remnant of radius ~ 100 pc at a distance of 20 Mpc occupies an angular diameter of $2''$ on the sky and could therefore be resolved. The strong emission lines from such a remnant can be detected with a signal-to-noise ratio of $S/N \approx 100$ after one hour of integration on the Keck telescope. Because of the temperature decrease at outer radii, we expect such a remnant to be center-filled in narrow-band imaging of high ionization lines (such as [O III] at 5007 Å or He II at 4686 Å), and limb-brightened for low-ionization lines (such as [S II] at 6717 Å). The non-relativistic blast wave does not reach the outer edge of young remnants, and might be visible in a deep exposure of a high resolution image. There might also be synchrotron emission in the radio band from the accelerated electrons in this shock. More interestingly, GRB remnants are expected to show ionization cones if the early UV afterglow emission from GRBs is beamed. The hydrodynamic spreading of the photo-ionized gas is negligible, as the gas expands at the sound speed of $\sim 10^2 \text{ km s}^{-1}$ and can traverse only a distance of $\lesssim 5$ pc ($t_L / 5 \times 10^4 \text{ yr}$) during the lifetime of the remnant. This distance is at least an order of magnitude smaller than the remnant radius, and so lateral expansion could smooth only extreme beaming factors of $f_b \lesssim (0.1^2 / 4\pi) = 10^{-3}$.

5. Conclusions

We have computed the emission spectrum which results from the cooling and recombination of an interstellar medium whose equilibrium state has been altered by a GRB and its subsequent afterglow emission. We have identified some generic signatures which are quite likely to bear the footprints of a GRB, and whose close study in nearby galaxies can in turn give us direct information on the sites where GRBs typically occur, and, maybe, lead us to the discovery of the remnant (if there is one) of the object which triggered the initial burst.

The X -ray emission is very weak compared to the UV and optical. This property could help separate GRBs from sources which provide a more steady energy supply, such as multiple supernovae or stellar winds; the latter type of sources tend to fill their remnants with hot X -ray emitting gas.

We have found that the $[\text{O III}]\lambda 5007$ to H_β line ratio is indicative of the high values of the ionization parameter in GRB remnants (see Figures 4 and 5). Detection of this and similar generic lines (cf. Figure 3) at a signal-to-noise ratio $S/N=100$ is feasible for remnants in the Virgo cluster after an hour of integration time with the Keck 10 meter telescope. Narrow-band imaging of such remnants could resolve the shock from the photoionized region inside these remnants, and should reveal ionization cones if the early (prompt or afterglow) UV emission from GRBs is beamed.

We thank John Huchra for useful discussions. AL and RP were supported in part by NASA grants NAG 5-7039 and NAG 5-7768. JR was supported in part by NASA grant NAG 5-2845.

REFERENCES

- Akerlof, C. W., et al. 1999, *Nature*, in press, astro-ph/9903271
- Anders, E., & Grevesse, N. 1989, *Geochim. Cosmochim. Acta*, 53, 197
- Baldwin, J. A., Phillips, M. M., & Terlevich, R. 1981, *PASP*, 93, 5
- Baum, S. A., Heckman, T. M. & van Breugel, W. 1992, *ApJ*, 389, 208
- Bloom, J. S., et al. 1999, astro-ph/9902182
- Böttcher, M., Dermer, C. D., Crider, A. W. & Liang, E. P., astro-ph/9809156
- Burgess, A. 1965, *ApJ*, 141, 1588
- Cox, D. P. 1972, *ApJ*, 178, 143
- Cox, D. P., Raymond, J. C. 1985, *ApJ*, 298, 651
- Dopita, M. A. & Sutherland, R. S. 1995, 455, 468
- Efremov, Y. N., Elmegreen, B. G., & Hodge, P. W. 1998, *ApJ*, 501, L163
- Fenimore, E. E. & Bloom, J. S. 1995, *ApJ*, 453, 25

- Fruchter, A. S., et al. 1998b, to appear in Proc. of the 4th Huntsville Symposium on Gamma-Ray Bursts, eds. C. A. Meegan, R. Preece, & T. Koshut, astro-ph/9801169
- Galama, T. J., et al. 1998, ApJL, 500, 101
- Ghisellini, G. et al. astro-ph/9808156
- Hartigan, P. Raymond, J. & Hartmann, L. 1987, ApJ, 316, 323
- Jacobs, V. L., Davis, J., Kepple, P. C., blaha, M. 1977, ApJ, 211, 605
- Loeb, A., & Perna, R. 1998, ApJ, 503, L35
- MacFadyen, A., & Woosley, S. E. 1998, ApJ, submitted, astro-ph/9810274
- Meszaros, P., & Rees, M. J. 1997, 476, 232
- Meszaros, P., & Rees, M. J. 1998, MNRAS, 299L, 10
- Morse, J. A. et a. 1996, AJ, 112, 509
- Paczynski, B., & Rhoads, J. E. 1993, ApJ, 418, L5
- Perna, R., Loeb, A. 1998, ApJ, 501, 467
- Raymond, J. C. 1979, ApJS, 39, 1
- Raymond et al. 1998, ApJ, 324, 869
- Reilman, R. F. & Manson, S. T. 1979, ApJ Suppl, 40, 815
- Rhode, K. L., Salzer, J. J., Westfahl, D. J., & Radice, L. 1999, AJ, in press, astro-ph/9904065
- Roach, F. E., & Gordon, J. L. 1973, The Light of the Night Sky, (Dordrecht: Reidel)
- Ruffert, M., & Janka, H.-Th. 1998, A & A, submitted, astro-ph/9809280
- Sari, R. 1997, ApJ, 489, L37
- Sedov, L. I. 1959, Dimensional Methods in Mechanics, (New York: Academic Press)
- Shull, J. M. & McKee, C. F. 1979, ApJ, 227, 131
- Vietri, M. 1997a, ApJ, 478L, 9
- Vietri, M. 1997b, ApJ, 488L, 105
- Younger, S. E. 1981, JQSRT, 26, 329
- Wang, Q. D. 1999, astro-ph/9903246
- Waxman, E. 1997a, ApJ, 485, L5
- Waxman, E. 1997b, ApJ, 489, L33
- Wijers, R. A. M., & Galama, T. J. 1998, ApJ, submitted, astro-ph/9805341
- Wijers, R. A. M. J., Rees, M. J., & Meszaros, P. 1997, MNRAS, 288, L51
- Wijers, R. A. M. J., Bloom, J. S., Bagla, J. S., & Natarajan, P. 1997, MNRAS,

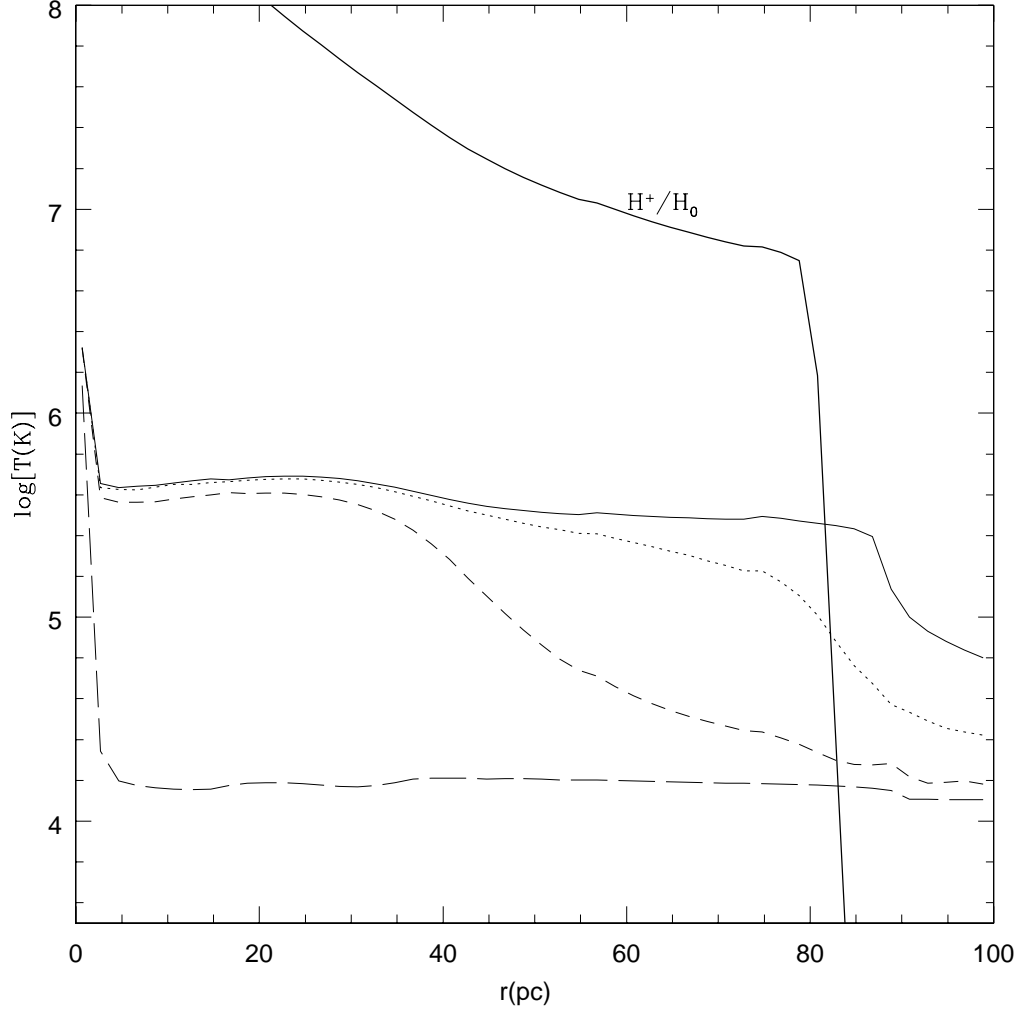


Fig. 1.a.— Temperature profile of the remnant of a GRB of energy 10^{52} ergs in a medium of density 1 cm^{-3} . Here the times are $t_{\text{obs}} = 3 \times 10^2$ yr (solid line), $t_{\text{obs}} = 3 \times 10^3$ yr (dotted line), $t_{\text{obs}} = 10^4$ yr (dashed line), $t_{\text{obs}} = 10^5$ yr (long-dashed line). The bold line shows the ionized hydrogen fraction H^+/H^0 at the times immediately following the passage of the afterglow radiation through the shells.

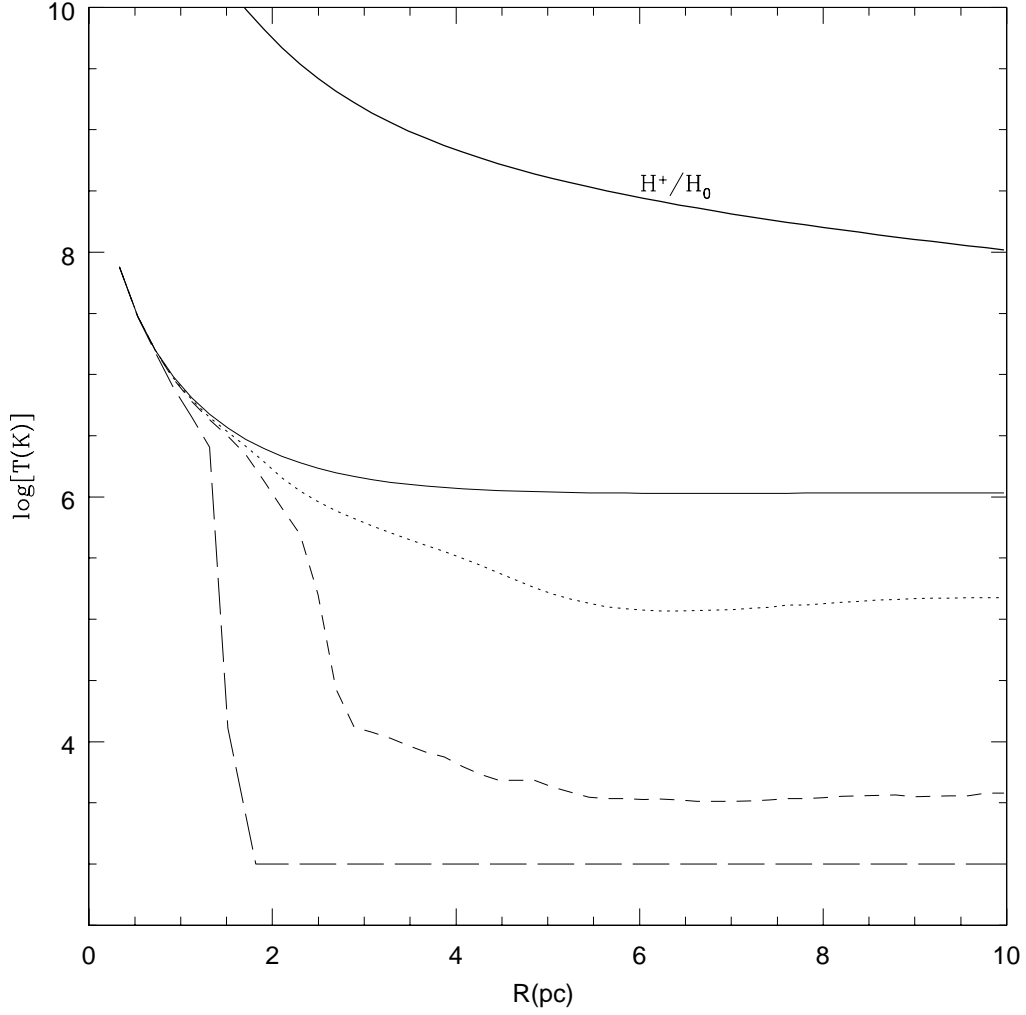


Fig. 1.b.— Temperature profile of the remnant of a GRB of energy 10^{52} ergs in a dense cloud of density 10^2 cm^{-3} and radius 10 pc. Here the times are $t_{\text{obs}} = 10 \text{ yr}$ (solid line), $t_{\text{obs}} = 10^3 \text{ yr}$ (dotted line), $t_{\text{obs}} = 2 \times 10^3 \text{ yr}$ (dashed line), and $t_{\text{obs}} = 10^4 \text{ yr}$ (long-dashed line). The bold line shows the ratio H^+/H^0 at the times immediately following the passage of the afterglow radiation through the shells.

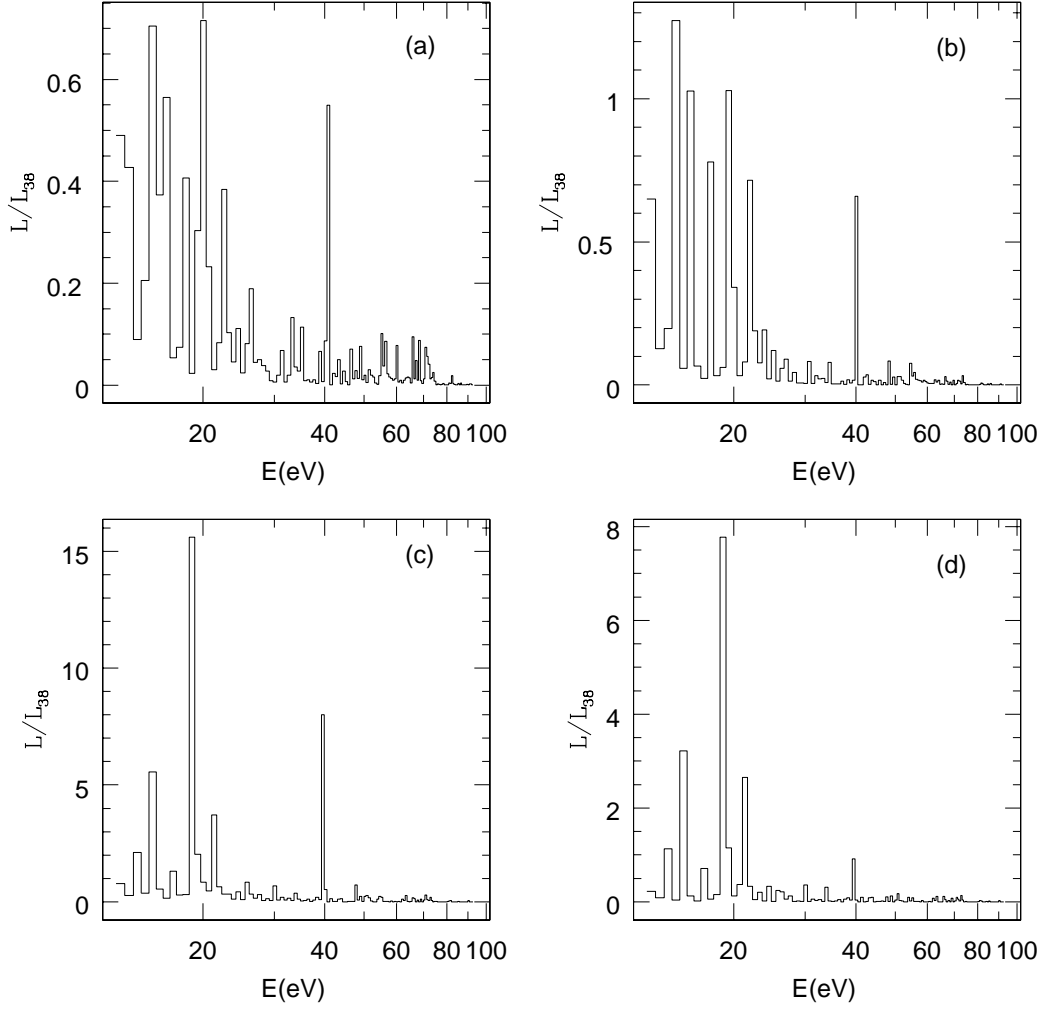


Fig. 2.a.— Emission spectrum above 13 eV of the remnant of a GRB of energy 10^{52} ergs in a medium of density 1 cm^{-3} . Here the times are $t_{\text{obs}} = 3 \times 10^2 \text{ yr}$ [panel (a)], $t_{\text{obs}} = 3 \times 10^3 \text{ yr}$ [panel (b)], $t_{\text{obs}} = 10^4 \text{ yr}$ [panel (c)], $t_{\text{obs}} = 10^5 \text{ yr}$ [panel (d)]. L_{38} is the luminosity in each photon-energy bin in units of $10^{38} \text{ erg sec}^{-1}$.

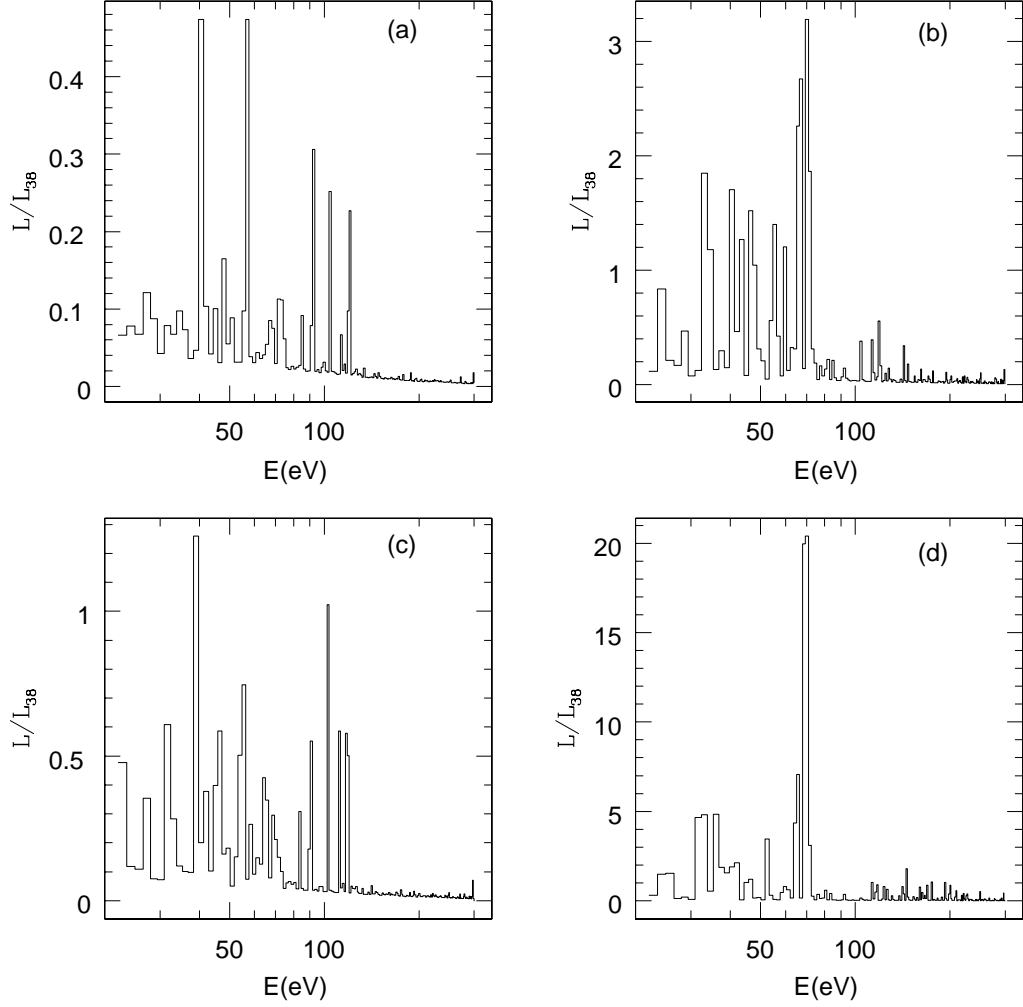


Fig. 2.b.— Emission spectrum above 13 eV of the remnant of a GRB of energy 10^{52} ergs in a dense cloud of density 10^2 cm^{-3} and radius 10 pc. Here the times are $t_{\text{obs}} = 30$ yr [panel (a)], $t_{\text{obs}} = 10^2$ yr [panel (b)], $t_{\text{obs}} = 2 \times 10^3$ yr [panel (c)], $t_{\text{obs}} = 2 \times 10^4$ yr [panel (d)].

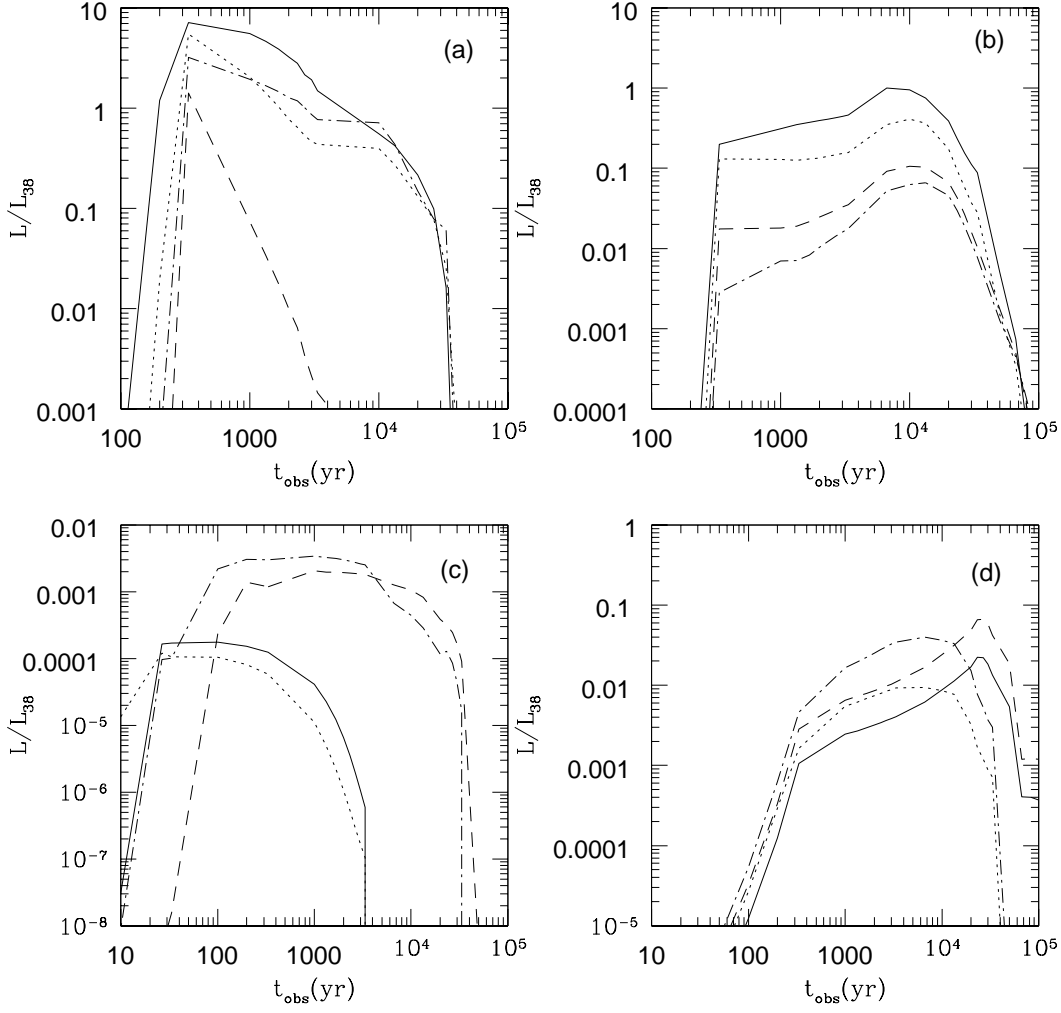


Fig. 3.a.— Time variation of the luminosity of some of the strongest emission lines for the remnant of a GRB of energy 10^{52} ergs in a medium of density 1 cm^{-3} . The lines are the following: in panel (a), He II at $\lambda = 1640\text{\AA}$ (dashed line), C III at $\lambda = 977\text{\AA}$ (dotted-dashed line), C IV at $\lambda = 1549\text{\AA}$ (dotted line), O VI at $\lambda = 1034\text{\AA}$ (solid line); in panel (b), [O III] at $\lambda = 4959+5007\text{\AA}$ (solid line), [O II] at $\lambda = 3729\text{\AA}$ (dotted line), [S II] at $\lambda = 6717\text{\AA}$ (dotted-dashed line), [N II] at $\lambda = 6548+6584\text{\AA}$ (dashed line); in panel (c), O VII at $\lambda = 21.60\text{\AA}$ (dashed line), O VIII at $\lambda = 18.97\text{\AA}$ (dotted-dashed line), Fe XXV at $\lambda = 1.859\text{\AA}$ (solid line), Fe XXVI at $\lambda = 1.780\text{\AA}$ (dotted line); in panel (d), $H\alpha$ (dashed line), $H_c\alpha$ (dotted-dashed line), $H\beta$ (solid line), $H_c\beta$ (dotted line).

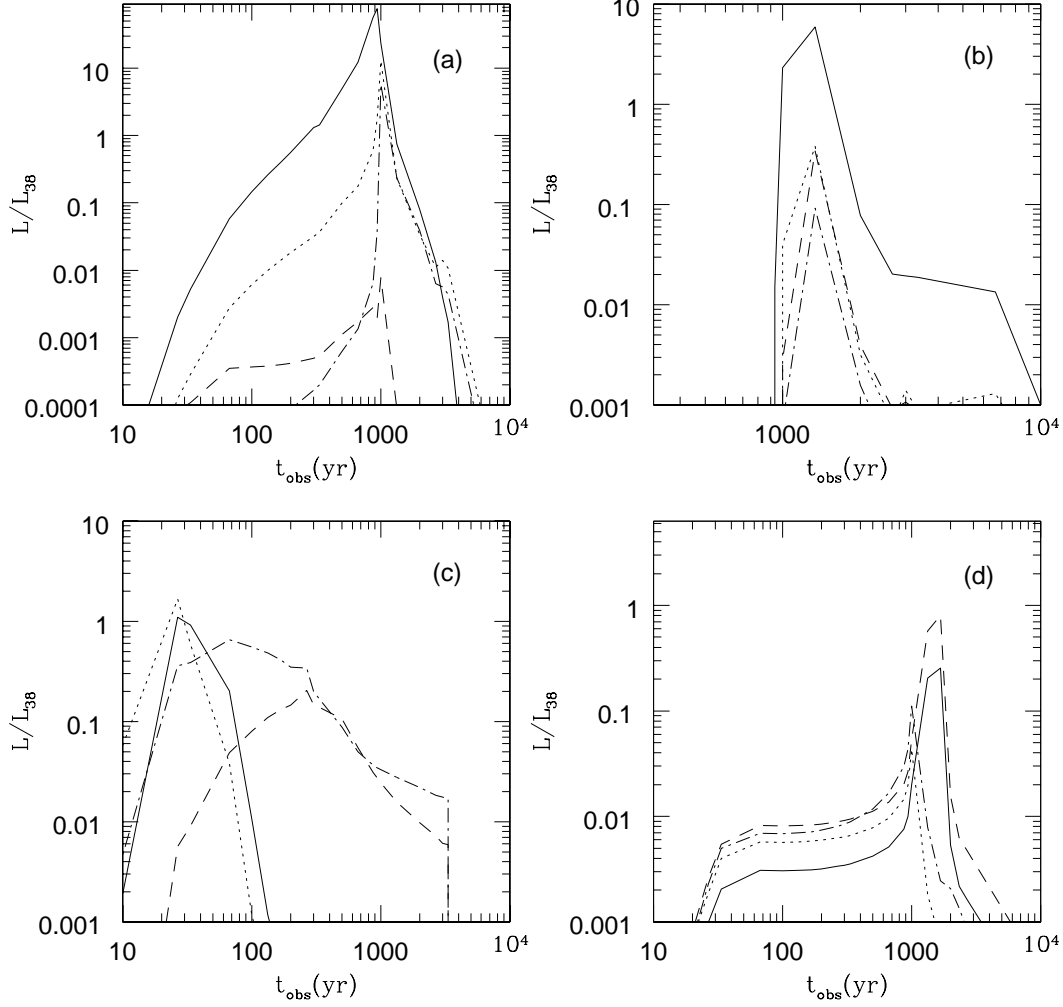


Fig. 3.b.— Time variation of the luminosity of some of the strongest emission lines for the remnant of a GRB of energy 10^{52} ergs in a molecular cloud of density 10^2 cm^{-3} and radius 10 pc. The lines are the same as in Figure 3a.

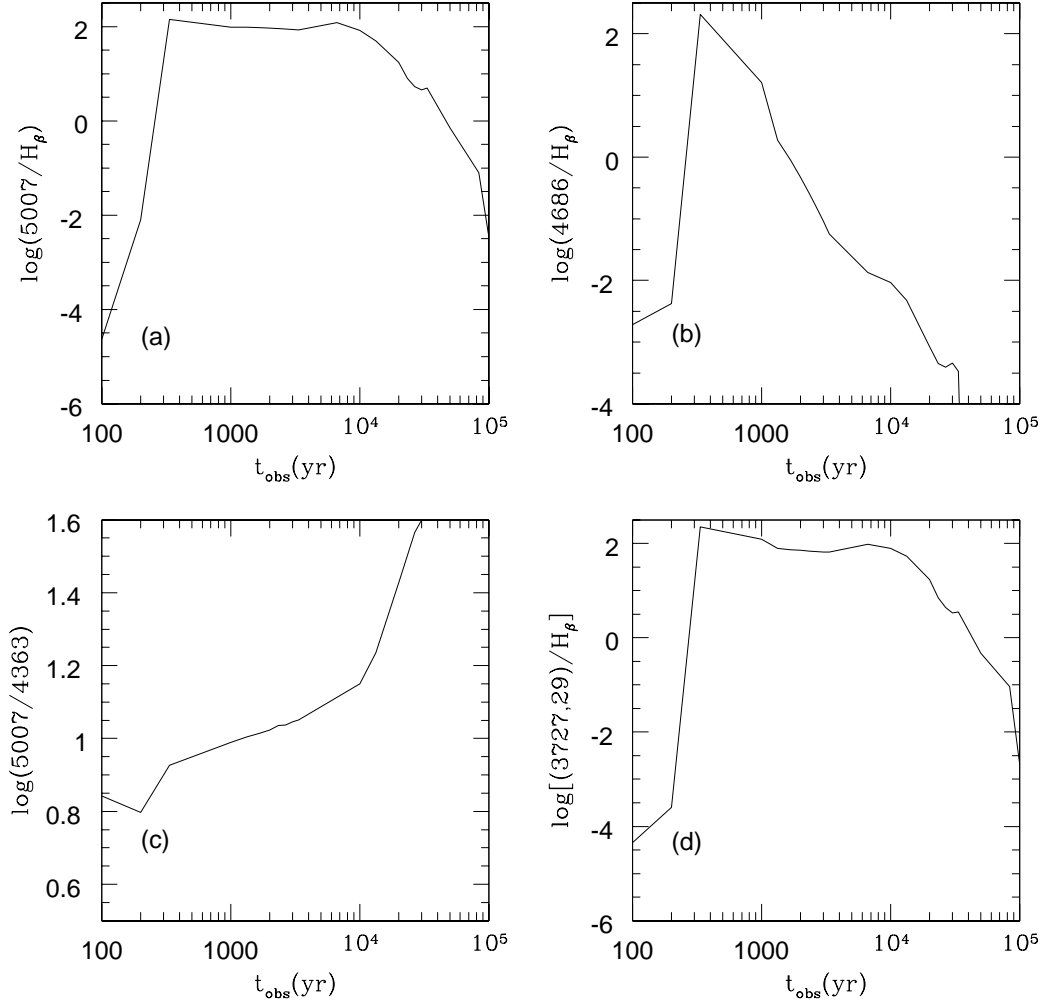


Fig. 4.a.— Time dependence of some line ratios that can be used as diagnostics for the remnant of a GRB of energy 10^{52} ergs in a medium of density 1 cm^{-3} .

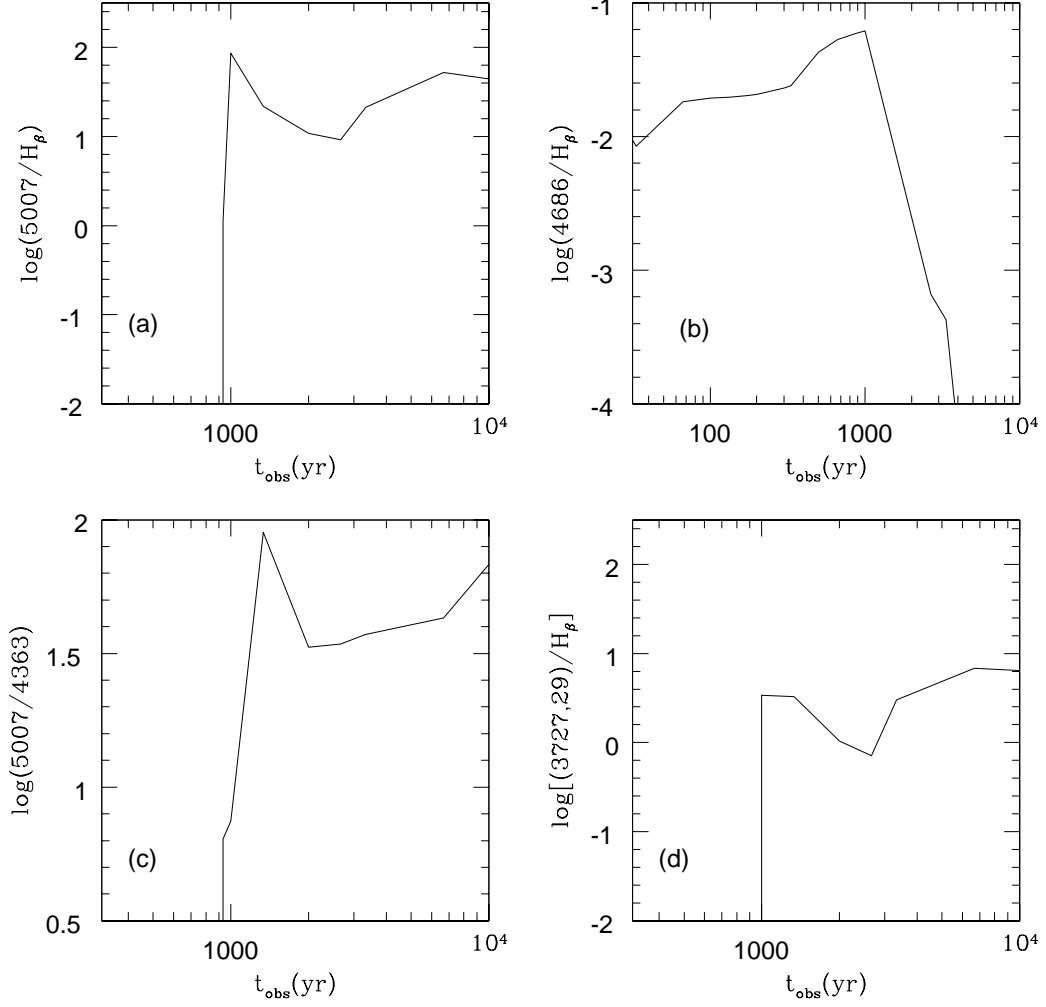


Fig. 4.b.— Same as in Figure 4a, but for the remnant of a GRB of energy 10^{52} ergs in a molecular cloud of density 10^2 cm^{-3} and radius 10 pc.

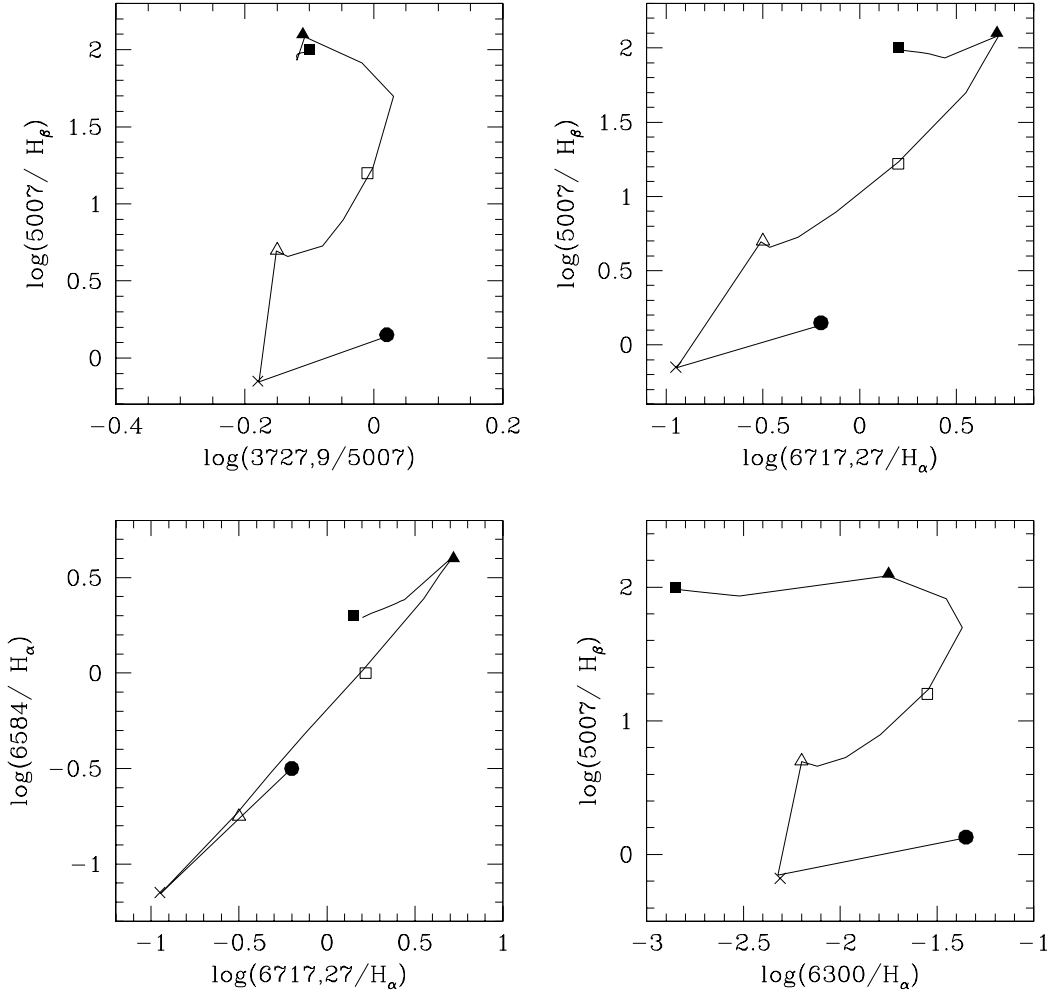


Fig. 5.a.— Line diagnostics for the remnant of a GRB of energy 10^{52} ergs in a medium of density 1 cm^{-3} . Here some of the times are indicated by a special symbol. In order, these are the correspondences: filled square: $t_{\text{obs}} = 10^3$ yr; filled triangle: $t_{\text{obs}} = 6 \times 10^3$ yr; empty square: $t_{\text{obs}} = 2 \times 10^4$ yr; empty triangle: $t_{\text{obs}} = 4 \times 10^4$ yr; cross: $t_{\text{obs}} = 5 \times 10^4$ yr; filled circle: $t_{\text{obs}} = 7 \times 10^4$ yr.

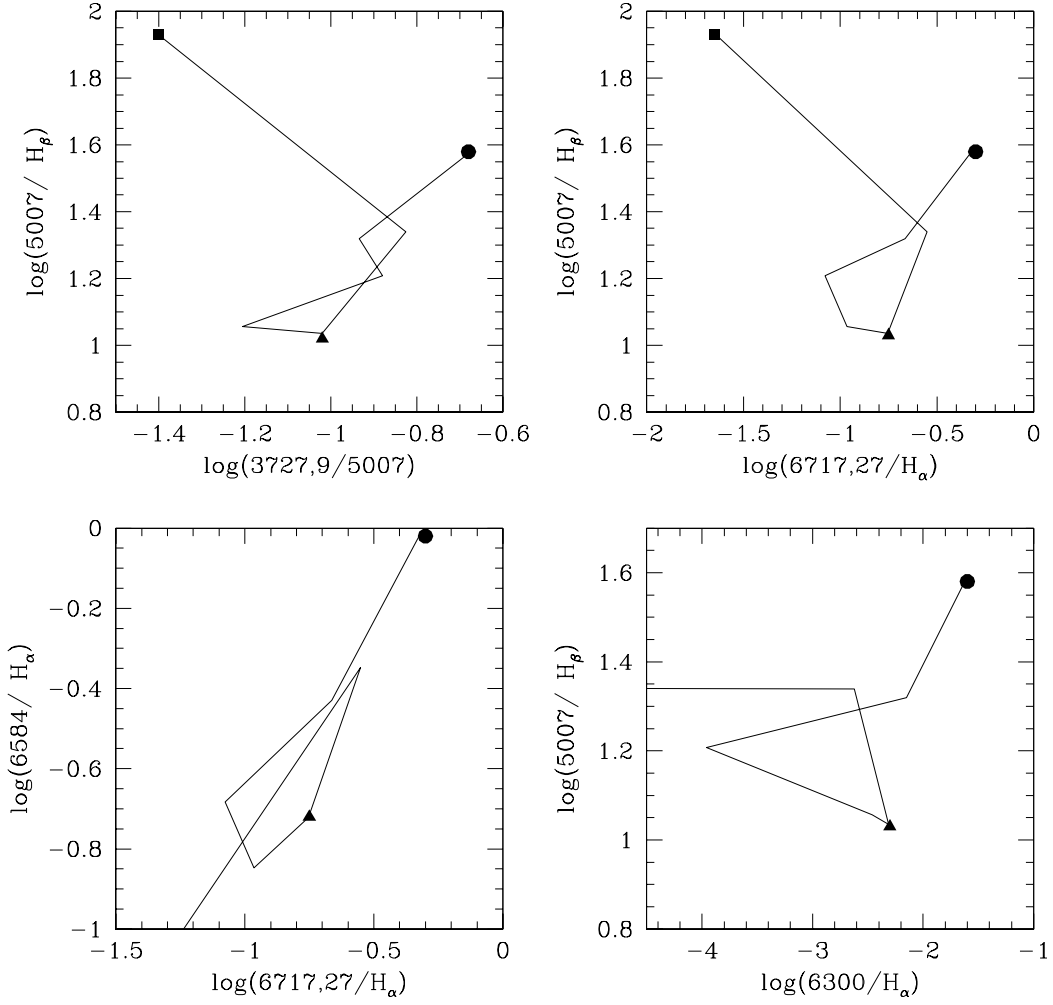


Fig. 5.b.— Same diagnostics as in Figure 5a, but for the remnant of a GRB of energy 10^{52} ergs in a molecular cloud of density 10^2 cm^{-3} and radius 10 pc. The times indicated here by a special symbol are the following: filled square: $t_{\text{obs}} = 10^3$ yr; filled triangle: $t_{\text{obs}} = 2 \times 10^3$ yr; filled circle: $t_{\text{obs}} = 7 \times 10^3$ yr.